

Short Communication

Corrosion Behaviour of Ti–6Al–4V Alloy as Dental Implant Containing Fluoride Ions

*Yingying Xu, Jing Wang, Xingle Zhang, Peng Wang, Jinghua Shi and Feng Huo**

Department of Stomatology, Affiliated Hospital of Chengde Medical University, Chengde, Hebei 067000, P.R. China

*E-mail: huofeng9876@163.com

Received: 15 July 2017 / Accepted: 26 August 2017 / Published: 12 October 2017

This work investigated the corrosion performance of Ti–15Mo alloy in NaCl (0.15 M) + NaF (different concentrations) and compared the protective capacity of this alloy and two other alloys (Ti–6Al–4V and CP-Ti) to ascertain their suitability for application in dental implanting. The Ti–6Al–4V, Ti–15Mo and CP-Ti alloys exhibited steady-state current densities of 6, 2 and 1 $\mu\text{A}/\text{cm}^2$, respectively, when investigated in NaCl (0.15 M) + NaF (0.03 M) at 200 mV (versus SCE). This result suggested desirable corrosion resistance of the three alloy samples in the potential range that could exist in the oral environment.

Keywords: Corrosion; Dental implant; Fluoride ions; Electrochemical study; Ti–6Al–4V alloy

1. INTRODUCTION

Titanium (Ti) and Ti-based alloys possess desirable mechanical characteristics, corrosion resistance and biocompatibility, along with low density, and thus have been extensively applied in dental and orthopaedic implants [1-3]. This is because desirable corrosion protection is supplied by the natural formation of a remarkably stable passive oxide layer (usually 4–6 nm) on them, which also possesses its own undesirable mechanical characteristics. Based on previous studies, shear stresses at extremely low levels (even rubbing by soft tissues) would lead to disruption of the naturally formed passive oxide layer. The passive oxide layer would be fractured under sliding and fretting wear conditions [4-9].

Regarding the fretting corrosion, the materials degrade at the contacting surface interfaces, since oscillatory movements of less than 100 μm between them with a corrosive intermediary occurred. Fretting corrosion is accepted in most types of dental, knee and hip implants [10]. In the case

of fretting corrosion with respect to orthopaedic implanting, wear debris could accumulate in the surrounding tissues, metal ions could be released into the human body, and the femoral stem could be loosened, thus leading to failure of the total joint prosthesis [11]. The fretting motion with respect to the dental implant is ordinarily caused by the biting force, or mastication on the abutment/ceramic crown or on the implant/abutment [8]. In the case of fretting corrosion, the skin could suffer reddening, toxicity and allergic reaction, the tissues could be inflamed, and so on [9]. Based on the literature, the tribocorrosion performance of original and modified stainless steel including CoCrMo, Ti-6Al-4V and CP-Ti alloys has been studied in simulated artificial saliva/body fluids [12-20]. The reports on *in vitro* tribocorrosion offer a desirable platform for understanding the stability of the passive film, the corrosion susceptibility of the material after removing the passive film, the destruction extent of the material, the property of the formed particulate debris, and the repassivation capacity. According to these investigations, mechanical forces are the primary influencing factors of the fracture of the passive oxide layer and the subsequent removal of this layer, the damage of the contact region, and the generation extent of the particulate debris. However, the corrosiveness of the medium is the main cause of the corrosion and repassivation of the material. Any mechanical force would lead to damage of the passive oxide layer on these materials. Therefore, repassivation is considered significant with respect to the stability of materials.

Recently, β -type Ti alloys (typical of Ti-Mo alloys) have been attractive as a biomaterial due to their desirable mechanical biocompatibility and corrosion resistance [21-23]. Ti-15Mo alloy was proposed among the potential biocompatible Ti-based alloys by Nag et al. [24], considering its strengthening mechanisms and microstructural development. According to Oliveira and co-workers [25] and Oliveira and Guastaldi [26], Ti-Mo alloys (Mo: 4-20 wt.%) not only are capable of spontaneous passivation in Ringer's solution but also avoid pitting at potentials as high as 8 V (versus SCE). Ti-Mo alloys have also been proposed by Oliveira and Guastaldi [26] as a proper biomaterial; since they are capable of spontaneous passivation, the passive films generated on these alloys exhibit favourable electrochemical stability, and this type of alloy is remarkably biocompatible. According to Kumar and Sankara Narayanan [21], Ti-15Mo alloy exhibited similar corrosion and pitting corrosion resistance to Ti-6Al-4V alloy, and better than CP-Ti alloy. Alves et al. [27] reported that Ti-10Mo alloy exhibited lower passive current density than Ti-6Al-4V alloy, despite their similar electrochemical properties in NaCl (0.15 M) + NaF (0.03 M). Alves-Rezende et al. [28] proposed that a steady state was rapidly reached for Ti-10Mo and CP-Ti alloys in the presence of NaF (0.05 wt.%), while a similar potential was reached slowly in commercial mouthwashes. Our previous reports [22] have presented the corrosion performance of Ti-15Mo alloy in NaCl (0.15 M) + NaF (different concentrations). The purpose of this work is to confirm the suitability of the three Ti-based alloys (specifically, Ti-6Al-4V, CP-Ti and Ti-15Mo alloys) when applied to dental implanting by assessing the corrosion performance of Ti-15Mo alloy and by comparing the corrosion protective capacity of the other alloys.

2. EXPERIMENTS

Ti-15Mo alloy was obtained as a gift specimen from the National Institute for Materials Research (NIMS), Japan. Ti-6Al-4V and CP-Ti (Grade 2) were commercially available in M/s Ti

Anode Fabricators, Chennai, India; the three alloys were used as received. The test specimens were cut from a 2 mm sheet, and applied for microstructural measurement, structural properties, and corrosion investigation. Table 1 presents the chemical composition of Ti–15Mo, Ti–6Al–4V and CP-Ti (Grade 2) alloys. An image analyser software application and a Leica DMLM optical microscope were used to evaluate the microstructure of the Ti-based specimens. The fabrication and etching procedures were presented in previous studies [21-23]. Cu-K α radiation was applied to X-ray diffraction (XRD) characterizations to assess the structural properties of these Ti-based alloys. The effect of fluoride was investigated by adding 0.01, 0.03, 0.06 and 0.5 M NaF into the base electrolyte, NaCl solution (0.15 M), to assess the corrosion performance of these Ti-based specimens. The NaF concentration and the base electrolyte were selected according to previous works [29, 30]. The concentration of fluoride (with respect to NaF) detected in some purchased prophylactic gels and toothpastes was found in a range of 0.1–2.0 (wt.%) [31]. Therefore, in this work, the effect of fluoride on the corrosion performance of these Ti-based specimens was investigated using NaF at varying concentrations (0.01, 0.03, 0.06 and 0.5 M).

Table 1. Chemical composition (wt. %) of the Ti alloys used in this work.

Element	Composition (wt.%)		
	CP-Ti	Ti-6Al-4V alloy	Ti-15Mo alloy
N	0.01	0.02	0.01
C	0.02	0.03	0.02
H	0.01	0.011	0.011
Fe	0.20	0.22	0.012
O	0.18	0.16	0.10
Al	—	6.12	—
V	—	3.93	—
Mo	—	—	15.03
Ti	Balance	Balance	Balance

The corrosion behaviour of Ti alloys was evaluated by performing chronoamperometric/current–time transient (CTT) and potentiodynamic polarization measurements. The working, auxiliary and reference electrodes were Ti or Ti alloy specimens, a graphite rod and a saturated calomel electrode (SCE), respectively. Only 1 cm² of the specimen was exposed to the electrolyte solution by placing the aforementioned electrodes in a flat cell in a certain way. The passivation performance was assessed by performing potentiodynamic polarization investigations based on open circuit potential (OCP) measurement in a range of –250 mV to +3000 mV (versus SCE), and the scan rate was 100 mV/min. The selected scan rate must be slow enough to represent only the interfacial corrosion process at every potential of the polarization scan, rather than the surface capacitance charging. Moreover, one must maintain a proper balance between the slow scan rates and rapidly obtaining the needed data. Furthermore, a similar scan rate must be maintained to guarantee a consistent comparison among varying alloys under certain conditions and vice versa.

In the present study, three varying potentials—+500 mV, +1250 mV and +2000 mV (versus SCE)—were applied to the CTT investigations. Due to the intraoral oxidation potential range of -58 mV to $+212$ mV (versus SCE), an impressed potential of $+200$ mV (versus SCE) was selected for the CTT investigations in 0.15 M NaCl that contained 0.03 M NaF for 0.5 h. We also presented a comparison in the behaviour of Ti–15Mo, Ti–6Al–4V and CP-Ti alloys based on the current density obtained in a steady state. The Ti-based specimens were exposed to a CTT investigation bed for 0.5 h at $+200$ mV (versus SCE) to study their surface morphology. All tests were performed in air at 27 ± 1 °C under static conditions. Many reports focused on the investigation of the corrosion performance of Ti and Ti-based alloys at 37 ± 1 °C (human body temperature), whereas several of them investigated the tribocorrosion and corrosion performance of Ti and Ti-based alloys at 24 – 30 °C (ambient temperature), as shown in a recently proposed review on the corrosion of alloys applied to dentistry.

3. RESULTS AND DISCUSSION

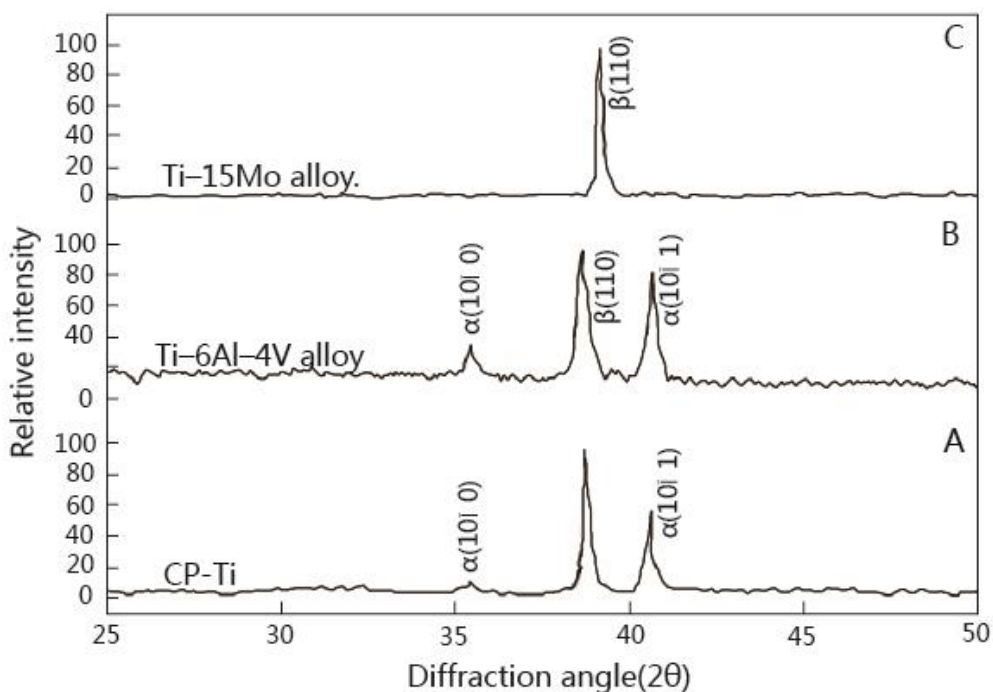


Figure 1. X-ray diffraction (XRD) profile of: (A) CP-Ti; (B) Ti–6Al–4V sample and (C) Ti–15Mo sample.

As shown in the XRD profiles, an entire hexagonal α -phase was observed for the CP-Ti sample in Fig. 1A. The XRD profile of Ti–6Al–4V sample displayed α - and β -phases, as shown in Fig. 1B. In addition, Ti–15Mo displayed only β -phase, as indicated by its XRD profile in Fig. 1C. The structural and microstructural properties of Ti and Ti-based alloys are mainly associated with the phase content and alloying elements in these alloys. The α - phase structure of the CP-Ti sample was excellently built

up, along with the $\alpha + \beta$ -phase structure of the Ti-6Al-4V sample. With respect to the retention of the β -phase in Ti-based alloys containing higher concentrations of Mo, a great amount of equiaxed β -phase was shown in Ti-Mo samples containing Mo (9 wt.%), while β -phase became the only primary phase in alloys that contained Mo of no less than ≥ 10 wt.%.

As displayed in Fig. 2A, the Ti-15Mo, Ti-6Al-4V and CP-Ti samples in NaCl (0.15 M) were characterized via potentiodynamic polarization profiles. In addition, Fig. 2B and 2C show the corresponding profiles after adding NaF (0.06 and 0.5 M, respectively) in NaCl (0.15 M). An active-passive transition was observed in the anodic branch of the polarization profiles for these Ti-based specimens. Due to the existence of H^+ , cathodic polarization is relieved, facilitating the electron flow to the cathode so that the corrosion process is enhanced; this is known as hydrogen depolarization corrosion [32]. The three Ti-based specimens all displayed an extension of the active region onto a higher current region in the polarization profiles after adding NaF to the electrolyte solution. Despite the active region increase, a passive film was observed after adding fluoride ions with additionally increased potential in the anodic direction for the three Ti-based specimens. Table 2 presents the corrosion parameters deduced from the potentiodynamic polarization curves.

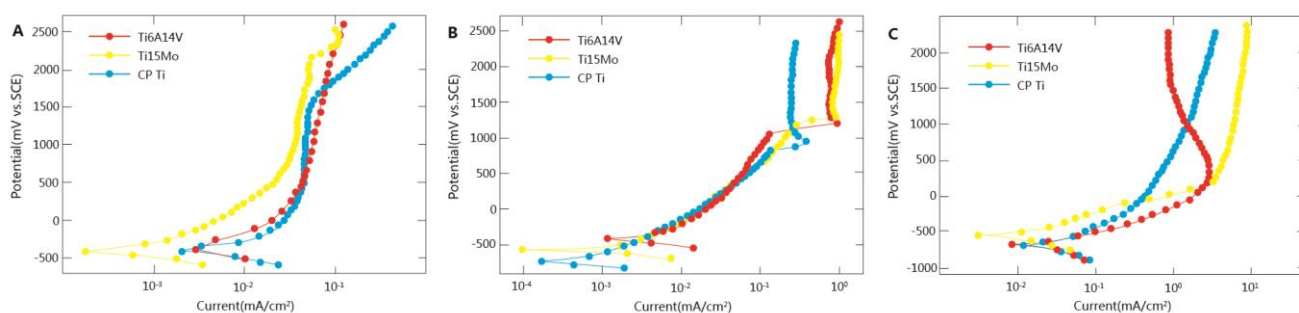


Figure 2. Potentiodynamic polarization profiles of CP-Ti, Ti-6Al-4V and Ti-15Mo samples in (A) NaCl (0.15 M); (B) NaCl (0.15 M) + NaF (0.06 M) and (C) NaCl (0.15 M) + NaF (0.5 M).

Table 2. Electrochemical polarization parameters for CP-Ti, Ti-6Al-4V and Ti-15Mo in three conditions.

Sample	E_{corr} (mV)	I_{corr} (mA/cm²)	b_a (mV/dec)	b_c (mV/dec)
NaCl (0.15 M)				
CP-Ti	-480	4.33	44	88
Ti-6Al-4V	-502	4.57	54	92
Ti-15Mo	-506	4.56	49	91
NaCl (0.15 M) + NaF (0.06 M)				
CP-Ti	-489	4.45	43	77
Ti-6Al-4V	-466	4.66	52	89
Ti-15Mo	-470	4.59	42	85
NaCl (0.15 M) + NaF (0.5 M)				
CP-Ti	-488	4.51	47	91
Ti-6Al-4V	-502	4.78	59	98
Ti-15Mo	-510	4.99	60	96

As indicated in the polarization profiles of Ti-15Mo, Ti-6Al-4V and CP-Ti samples, the passive region corresponded to the formation of no less than one protective oxide film, while the active region corresponded to the formation of a defective/porous oxide layer and the electrochemical reaction of the specimen present in the electrolyte solution. An increase in the corrosion current density of the specimen of steel was observed when the NaF concentration was increased. It can be seen in Table 2 that compared to the low NaF concentration environment, the high H₂S concentration environment corrosion potential E_{corr} revealed a positive displacement from -506 mV to -510 MV. This displacement results from the decomposition effects on the substrate contributed by NaF [33-36]. Through XPS measurement, Huang [31] observed that Na₂TiF₆ formed on the surface of a Ti-6Al-4V specimen when immersed in pH 5 artificial saliva with + NaF (0.1 wt.%). Obviously, fluoride ions would be incorporated into the passive oxide layer of Ti and Ti-based alloys after adding NaF into NaCl (0.15 M), and then a porous layer would be formed. Therefore, it can be seen that the active region of the three Ti-based specimens with fluoride ions in this work increased, since a defective/porous oxide layer was formed.

Although the active region increased, a passive film formed with fluoride ions was shown for the three alloy specimens. HF was considered to contribute to the destruction of the passive oxide film formed on Ti and Ti-based specimens, and the HF concentration was reversely dependent on the pH of the medium. Upon the destruction of the passive oxide layer formed on Ti by the attack of fluoride, the regeneration rate of the passive oxide layer was a linear function of the concentration of the dissolved oxygen [37]. Therefore, we shall consider the combined effect of the concentration and pH value of NaF and the dissolved oxygen. This work used a NaF concentration range of 0.01–0.5 M in air, along with an only slightly acidic electrolyte medium (pH, 6.0). The HF concentration would be much lower than 30 ppm (0.003 wt.%), considering that the pH value of the test electrolyte solution was 6.0. The adequate concentration of dissolved oxygen was available, ; this could make the passive oxide layer regenerate on all Ti specimens tested in the present study, which would have been damaged by the attack of fluoride. The results of the transient of the present study further confirm the observations of other researchers [38, 39].

As shown in the literature, the passive current densities of Ti and Ti-based alloys depend on the concentration of NaF in the electrolyte. The open-circuit potentials then increased and reached noble values that characterize passive, resistant metals. E_{oc} values, including those from doping with 0.5M NaF saliva, were placed in the passive potential range of Ti [40, 41]. In addition, the Ti-6Al-4V specimen showed a passive current density increase with increasing concentration of fluoride ions in the electrolyte. The CP-Ti showed a lower average passive current density than the other specimens, ascribed to the fluoride ion-induced dissolution of the alloying elements. Ti-6Al-4V and Ti-15Mo specimens showed little change in the average passive current density in NaCl (0.15 M) + NaF (0.01 and 0.03 M). Compared with the Ti-6Al-4V specimen, the Ti-15Mo specimen showed higher passive current density in NaCl (0.15 M) + NaF (0.06 M). Nevertheless, compared with the Ti-6Al-4V specimen, the other two specimens showed much higher average passive current densities in NaCl (0.15 M) + NaF (0.5 M).

The behaviour of Ti-6Al-4V, Ti-15Mo and CP-Ti specimens in the present study was compared at intraoral oxidation potential via CTT investigations carried out at +200 mV (versus SCE)

in NaCl (0.15 M) + NaF (0.03 M) for 0.5 h, as indicated in Fig. 3. The three specimens showed steady-state current densities of 6, 2 and 1 $\mu\text{A}/\text{cm}^2$, respectively, at intraoral oxidation potential of +200 mV (versus SCE). The healing of corrosion initiation sites, which can be pores and cracks, seemed to occur by volume expansion through the hydration process of the anodic oxide films [42]. As shown in the current density range, the three specimens can offer improved corrosion resistance when exposed to the potential range that could be present under oral conditions. It can be seen that Ti-15Mo and CP-Ti specimens showed higher corrosion protective capacity, while the Ti-6Al-4V specimen exhibited comparatively lower protective capacity.

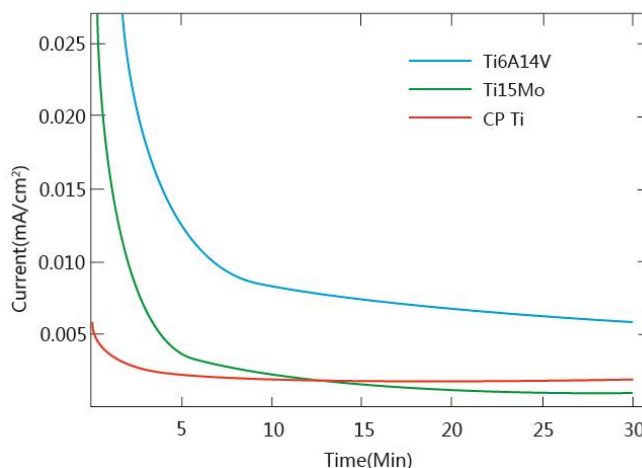


Figure 3. CTT profiles of CP-Ti, Ti-15Mo and Ti-6Al-4V samples in 0.15 M NaCl that contained 0.03 M NaF at 200 mV (versus SCE).

4. CONCLUSIONS

In this work, we assessed the corrosion performance of the Ti-15Mo specimen in NaCl (0.15 M) + 0.01, 0.03, 0.06 and 0.5 M NaF. To check whether the three alloy samples were suitable for application in dental implant utilities, we also compared the aforementioned specimen with the other specimens in terms of their corrosion behaviour. Compared with Ti-6Al-4V and CP-Ti specimens, the Ti-15Mo specimen also displayed a passive film formed with fluoride ions present in the electrolyte (as high as 0.5 M). The passive current density was found to significantly depend on the concentration of NaF present in the electrolyte. To be specific, the passive current density increased with the increasing NaF concentration.

ACKNOWLEDGEMENT

This work was supported by grants from The Chengde Science and Technology Support Program (NO.201601A025).

References

1. M. Long and H.J. Rack, *Biomaterials*, 19 (1998) 1621.
2. X. Liu, P.K. Chu and C. Ding, *Materials Science and Engineering: R: Reports*, 47 (2004) 49.

3. M. Geetha, A. Singh, R. Asokamani and A. Gogia, *Progress in materials science*, 54 (2009) 397.
4. R. Thull and M. Schaldach, Corrosion of highly stressed orthopedic joint replacements, *Engineering in Medicine*, Springer1976, pp. 242.
5. S.A. Brown, P.J. Hughes and K. Merritt, *Journal of orthopaedic research*, 6 (1988) 572.
6. D.W. Hoepfner and V. Chandrasekaran, *Wear*, 173 (1994) 189.
7. L.M. Rabbe, J. Rieu, A. Lopez and P. Combrade, *Clinical Materials*, 15 (1994) 221.
8. M. Barry, D. Kennedy, K. Keating and Z. Schauerperl, *Materials & design*, 26 (2005) 209.
9. M.H. Zhu, Z.B. Cai, W. Li, H.Y. Yu and Z.R. Zhou, *Tribology International*, 42 (2009) 1360.
10. B. Sivakumar, S. Kumar and T.S. Narayanan, *Wear*, 270 (2011) 317.
11. S.C. Jani, W.L. Sauer, T.W. McLean, R.D. Lambert and P. Kovacs, Fretting corrosion mechanisms at modular implant interfaces, *Modularity of Orthopedic Implants*, ASTM International1997.
12. F. Galliano, E. Galvanetto, S. Mischler and D. Landolt, *Surface and Coatings Technology*, 145 (2001) 121.
13. J. Geringer, B. Forest and P. Combrade, *Wear*, 259 (2005) 943.
14. M. Azzi and J.A. Szpunar, *Biomolecular engineering*, 24 (2007) 443.
15. S. Barril, S. Mischler and D. Landolt, *Wear*, 259 (2005) 282.
16. S. Xulin, A. Ito, T. Tateishi and A. Hoshino, *Journal of Biomedical Materials Research Part A*, 34 (1997) 9.
17. Z. Quan, P.-Q. Wu, L. Tang and J.P. Celis, *Appl. Surf. Sci.*, 253 (2006) 1194.
18. P.-Q. Wu and J.P. Celis, *Wear*, 256 (2004) 480.
19. S. Kumar, B. Sivakumar, T.S.N.S. Narayanan, S.G.S. Raman and S.K. Seshadri, *Wear*, 268 (2010) 1537.
20. A.C. Vieira, A.R. Ribeiro, L.A. Rocha and J.-P. Celis, *Wear*, 261 (2006) 994.
21. S. Kumar and T.S.N.S. Narayanan, *J. Alloy. Compd.*, 479 (2009) 699.
22. S. Kumar and T.S.N.S. Narayanan, *journal of dentistry*, 36 (2008) 500.
23. W.F. Ho, C.P. Ju and J.H.C. Lin, *Biomaterials*, 20 (1999) 2115.
24. S. Nag, R. Banerjee and H.L. Fraser, *Materials Science and Engineering: C*, 25 (2005) 357.
25. N.T.C. Oliveira, G. Aleixo, R. Caram and A.C. Guastaldi, *Materials Science and Engineering: A*, 452 (2007) 727.
26. N.T.C. Oliveira and A.C. Guastaldi, *Corrosion Science*, 50 (2008) 938.
27. A.P.R. Alves, F.A. Santana, L.A.A. Rosa, S.A. Cursino and E.N. Codaro, *Materials Science and Engineering: C*, 24 (2004) 693.
28. M.C.R. Alves Rezende, A.P.R. Alves, E.N. Codaro and C.A.M. Dutra, *Journal of Materials Science: Materials in Medicine*, 18 (2007) 149.
29. A.M. Al-Mayouf, A.A. Al-Swayih, N.A. Al-Mobarak and A.S. Al-Jabab, *Mater. Chem. Phys.*, 86 (2004) 320.
30. M.V. Capela, H.A. Acciari, J.M.V. Capela, T.M. Carvalho and M.C.S. Melin, *J. Alloy. Compd.*, 465 (2008) 479.
31. H.-H. Huang, *Biomaterials*, 24 (2003) 275.
32. C.G. Wang, *Materials Science Forum*, 852 (2016) 90.
33. W. Xue, X. Yang, J. Qiu, H. Liu, B. Zhao, H. Xia, X. Zhou, P. Huai, H. Liu and J. Wang, *Corrosion Science*, 114 (2017) 96.
34. T.T. Bataineh, M.A. Al-Qudah, E.M. Nawafleh and N.A. Al-Rawashdeh, *Int. J. Electrochem. Sci.*, 9 (2014) 3543.
35. J. Xu, Q. Yang, M.S. Javed, Y. Gong, M.K. Aslam and C. Chen, *RSC Advances*, 7 (2017) 5880.
36. J.M.C. Moreno, M. Popa, S. Ivanescu, C. Vasilescu, S.I. Drob, E.I. Neacsu and M.V. Popa, *Metals and Materials International*, 20 (2014) 177.
37. M. Nakagawa, S. Matsuya and U. Koich, *Dental Materials Journal*, 20 (2001) 305.
38. A. Al-Mayouf, A. Al-Swayih, N. Al-Mobarak and A. Al-Jabab, *Materials Chemistry and Physics*, 86 (2004) 320.

39. A. Alves, F. Santana, L. Rosa, S. Cursino and E. Codaro, *Materials Science and Engineering: C*, 24 (2004) 693.
40. M. Hatami, M. Yeganeh, A. Keyvani, M. Saremi and R. Naderi, *Journal of Solid State Electrochemistry*, 21 (2017) 777.
41. M.M. Alves, D.V. Cunha, C.F. Santos, N.P. Mira and M.F. Montemor, *Journal of Materials Chemistry B*, 4 (2016) 4754.
42. M. Saremi and S.H. Mortazavi, *Micro & Nano Letters*, 11 (2016) 866

© 2017 The Authors. Published by ESG (www.electrochemsci.org). This article is an open access article distributed under the terms and conditions of the Creative Commons Attribution license (<http://creativecommons.org/licenses/by/4.0/>).